doi.org/10.1002/batt.202000189

Designing High-Performant Lithium Battery Electrolytes by Utilizing Two Natures of Li^+ Coordination: LiTDI/LiTFSI in Tetraglyme

Piotr Jankowski,*[a, b, c] Rasmus Andersson,[a] and Patrik Johansson[a, d]

Highly concentrated electrolytes (HCEs) based on glymes, such as tetraglyme (G4), are currently the focus of much battery research, primarily due to their unique properties – especially with respect to ion transport and electrochemical stability. While the LiTFSI-G4 and LiTDI-G4 systems both have been studied extensively, we here design their hybrid electrolytes to answer; will the resulting properties be averages/superpositions or will there be synergies created? We find the latter to be true and demonstrate that the most performant electrolytes are obtained by introducing a minor amount of LiTDI to an LiTFSI based electrolyte, which promotes the disproportionation and formation of "free" cations and at the same to avoid large aggregates – shown comprehensively both experimentally and by different modelling approaches and analyses combined. This electrolyte composition strategy can be generalized to other salts and solvents and thus a route towards a flora of novel battery electrolytes is here suggested.

1. Introduction

There is an urgent need for novel advanced electrolytes for lithium batteries combining fast ion transport with enhanced overall safety, reduced toxicity and improved thermal stability, *etc.*[1] Basically, the development of novel liquid electrolytes involves changes of only a few variables: molecular structure and ratio of salt(s) and solvent(s) and the special additives chosen and needed to create a functional electrolyte.[2–4] For the solvents the main interest has been and still is on ethers and esters, but many different lithium salts have been proposed and tested in the efforts to eliminate/reduce the problematic use of the $LiPF_6$ salt – the source of most disadvantages of the today prevalent standard LIB electrolytes such as LP40.[5,6] Here we focus on two of the most attractive candidates that have been suggested due to their combined transport and electrochemical properties as well as easy and upscalable synthesis: lithium bis(trifluoromethanesulfonyl)imide (LiTFSI)[7] and lithium 2-trifluoromethyl-4,5-dicyanoimidazole (LiTDI).[8] Indeed, both have been proposed for next generation lithium batteries.[9–11] One particular route explored for these Li-salts is a sub-class of highly concentrated electrolytes (HCEs)[12] based on the use of cation chelating ethers, glymes (CH_3–$(OC_2H_4)_n$–OCH_3: Gn, $n = 1$–6), as solvents to create solvate ionic liquids (SILs).[13] SILs are created by the very flexible Gn backbones, enabling them to adapt conformations and M^{x+}-O_{ether} coordinations to maximize the interactions and create a "soft" cationic supramolecular complex from a "hard" cation. This results in materials with high thermal stability, low volatility and high ionic conductivity – if the right choice of glyme is made for the cation, for Li^+ it is usually G3 or G4.[14] The formation of an SIL is, however, also highly dependent on the anion used – strong cation-anion interactions compete with/limit the cation-solvent interaction and lead to aggregation.[15] Also the structural rigidity or flexibility of the anion employed has a large impact; a flexible anion, *e.g.* TFSI, may allow for structural adjustments, while a rigid, *e.g.* TDI, may cause steric hindrances.[16] Combined this has huge consequences for the resulting local structure and the overall properties of the electrolytes where the TFSI-based tend to create SILs with weak cation-anion interactions via solvated ion-pairs, while the TDI-based tend to form polyanionic aggregates and "free" and mobile cationic species via a disproportionation mechanism.[16–18] The nature of the lithium cation solvation and transport is thus very different. Here we create and study in detail a wide range of hybrid LiTDI/LiTFSI HCEs by employing tetraglyme (G4) as solvent in order to elucidate any possible structural and/or dynamic synergies.

By varying both the LiTDI:LiTFSI ratio (from 0:10 to 10:0, *i.e.* $x_{TDI} = 0.0$–1.0) as well as the total salt to solvent ratio (1:1, 1:0.75, 1:0.5) we constructed 33 HCEs (Scheme 1) and assessed their phase-behaviour and the resulting ion conductivities. These properties are subsequently connected to the Li^+ coordination and the overall speciation – as elucidated by

[a] *Dr. P. Jankowski, R. Andersson, Prof. P. Johansson*
Chalmers University of Technology
Department of Physics
412 96 Gothenburg, Sweden
[b] *Dr. P. Jankowski*
Technical University of Denmark
Department of Energy Conversion and Storage
2800 Kgs. Lyngby, Denmark
E-mail: pioja@dtu.dk
[c] *Dr. P. Jankowski*
Warsaw University of Technology
Faculty of Chemistry
00-664 Warsaw, Poland
[d] *Prof. P. Johansson*
Alistore – European Research Institute
CNRS FR 3104, Hub de l'Energie
15 Rue Baudelocque, 80039 Amiens, France

Supporting information for this article is available on the WWW under https://doi.org/10.1002/batt.202000189

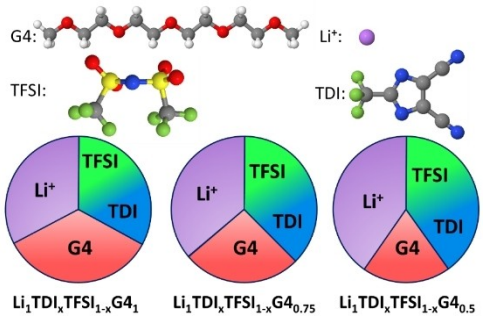

Scheme 1. Compositions of the mixed electrolytes.

vibrational spectroscopy as well as density functional theory (DFT) calculations and molecular dynamics (MD) simulations.

Experimental and Computational Section

All electrolytes were prepared inside an Ar-filled glovebox ($H_2O<$ 1 ppm, $O_2<10$ ppm) by mixing appropriate amounts of LiTDI (synthesized and dried as described earlier)[8] and LiTFSI (Solvionic, 99.9%). After short mixing of the white powders, tetraglyme (G4) (Sigma-Aldrich, 99%) was added in an appropriate amount and the mixtures were heated up to 150 °C upon intense stirring. For ion conductivity measurements, the electrolytes were placed between two stainless steel electrodes separated by a Teflon spacer in a coin cell geometry inside the glovebox. A Novocontrol broad-band dielectric spectrometer was used in the frequency range 10^{-1}–10^{7} Hz for measurements between 120 and −20 °C every 10 °C. The thermal data were recorded on a DSC250 (TA instruments) differential scanning calorimeter in the temperature range −150 °C–+ 150 °C. Samples were put in aluminium pans and conditioned at room temperature (≈20 °C) over one week to allow for any possible slow crystallization. All measurements were made using a scan rate of 10 °C min^{-1} in the sequence cooling-heating-cooling – and the heating traces are reported. The FT-IR spectra were collected on a Bruker Alpha inside the glovebox, using an ATR accessory with a diamond crystal and a spectral resolution of *ca.* 2 cm^{-1}. The Raman spectra were obtained using samples in glass vials taken out from the glovebox on a Bruker MulitiRAM FT Raman spectrometer with a 1064 nm Nd:YAG laser fitted with a liquid-N_2-cooled Ge-diode detector, and collected over 2000 scans with *ca.* 2 cm^{-1} spectral resolution.

DFT calculations were performed using the M06-2X functional and the 6–311++G(d,p) basis set, as implemented in Gaussian 16.[19] The interaction energies within the aggregates were calculated in the gas phase from the differences in electronic energy between separated ions and the aggregate, all in optimized geometries. The MD simulations were performed using the GROMACS package[20] with the OPLS-based force-field, as previously.[16] 21 systems were created with $x_{TDI}=0.0$, 0.1, 0.3, 0.5, 0.7, 0.9 and 1.0 and the salt to solvent ratios of 1:1, 1:0.75 and 1:0.5. The systems all contained 80 Li-salt molecules and were subsequently energy minimized and simulated under NVT and NPT conditions to obtain the starting geometries, followed by equilibration at 303 K for 20 ns. The MD production runs were 50 ns long using a time-step of 2 fs and a leapfrog algorithm under NPT and periodic boundary conditions at 1 bar and a V-rescale thermostat (coupling time 0.5 ps) and a Parrinello-Rahman barostat (coupling time 2 ps). A particle-mesh Ewald summation routine was used for the long-range forces (cut-off 12 Å). The SHAKE algorithm was used to constrain bonds involving hydrogen. The partial radial distribution functions (RDFs) and coordination numbers (CNs) involving Li^+, anions and G4 were computed using the MDanalysis package.[21] The CHAMPION analysis toolkit[22,23] was used to perform a deeper study of the global and local structure, as well as of the diffusive transport, for a few of the electrolytes; three of the least concentrated (1:1 salt: solvent) systems ($x_{TDI}=0.0$, 0.3, 1.0). The time-dependent covalent and coordination bonds were detected based on the atomic trajectories and used to construct bond graphs, from which connected components (*i.e.* ions, molecules, ion-pairs, aggregates, and networks) as well as Li^+ first solvation shells, were extracted and analysed by statistical physics, following a methodology presented elsewhere.[22,23] The Li^+ first solvation shells were distinguished based on the bond topologies up to two bonds (including both covalent and coordination bonds) away from the central Li^+ ion. The size distributions of connected components containing Li^+ were quantified by their cumulative distribution functions (CDFs) for the number of exemplars of each species, with CDF(n) denoting the probability of a Li^+ containing connected component having at least n exemplars of the respective species (Li^+, TDI, TFSI, G4). Species diffusivities were computed using mean squared displacements (MSDs) and decomposed into contributions from vehicular and structural transport mechanisms, with vehicular transport here defined as centre-of-mass motion of the connected component of a Li^+ ion and structural transport defined as motion relative to the former, and analogously for first solvation shell topologies. Based on this, cation transport numbers were computed as the fraction of total ionic conductivity carried by Li^+ ions: $t_{Li+} = D_{Li^+}/(D_{Li^+} + D_{X^-})$. A decomposition was also performed of the total Li^+ diffusivity into different first solvation shell topologies. Finally, the effective diffusivities of these topologies were computed by dividing their contribution to Li^+ transport by the probability of Li^+ being in each topology.

2. Results and Discussion

We start by investigating the phase stability and ionic conductivity as a function of both temperature and electrolyte composition and continue by studying the interactions and resulting speciation of ion-pairs and smaller ionic aggregates by computing energies of formation and disproportionation using DFT, which subsequently are compared to and corroborated by Raman and IR spectroscopy data. Finally, we use MD simulations extensively to get a more detailed view of both the global and local structure as well as the dynamics and the ion transport mechanisms of the electrolytes.

2.1. Phase Stability and Ionic Conductivity

As any HCEs may be prone to slow phase transitions from their sluggish kinetics due to the very high viscosities, calorimetric studies to detect any crystallinity were made one week after mixing. Apart from the electrolytes with an equimolar salt to solvent ratio, which all were completely amorphous, an increased salt to solvent ratio can cause partial crystallization for $x_{TDI}>0.4$ – with melting points observed above 100 °C (Figure S1). The time-frame of one week is admittedly ambiguous and we cannot be sure if also some of the equimolar salt to solvent ratio materials and/or materials with lower LiTDI

contents would crystallize with time. However, in a practical Li battery cell set-up using these kind of electrolytes this would be mitigated by designated thermal protocols – if needed. All electrolytes have glass transition temperatures in the range −80–−40 °C. Overall, the aggregation caused by TDI can lead to appearance of some crystalline phase and also a lowered ion conductivity of the LiTDI:G4 electrolytes as compared to LiTFSI:G4. The mixed electrolytes, however, offer some synergies; the relative ion conductivities show that at low temperatures the maximum ion conductivity is observed for $x_{TDI} \approx 0.3$–0.4 and upon increasing temperature there are three different trends observable: *i)* for the lowest total Li-salt content the maximum shifts to lower x_{TDI}, *ii)* for the highest to higher x_{TDI}, and *iii)* for the intermediate system the maximum remains stable at $x_{TDI} = 0.3$ (Figure 1, S2). From the general appearance of the heat-maps, we can deduce that a reduction of G4 in the electrolyte composition leads to an eutectic composition close to equimolar LiTFSI:LiTDI content. Moving to absolute numbers, an increased total Li-salt content decreases the ionic conductivity *e.g.* from $1.3 \cdot 10^{-3}$ S cm^{-1} to $1.3 \cdot 10^{-4}$ S cm^{-1} and $6.8 \cdot 10^{-4}$ S cm^{-1}, respectively, at 20 °C. The most striking feature is though what happens as a function of x_{TDI}; *vs.* the pure LiTFSI:G4 systems the optimal x_{TDI} offers higher ion conductivities by 22 %, 62 % and 1000 %. A one-order of magnitude improvement is thus observed for the most concentrated system.

2.2. Interaction and Speciation Studies

In order to understand the rationale of the synergies observed between LiTDI and LiTFSI at least two major fundamental aspects have to be considered: (i) the cation-anion interactions, *i.e.* Li^+-TDI and Li^+-TFSI – including the role of G4 encapsulated Li^+, $[LiG4]^+$, and (ii) the cation-solvent interactions, *i.e.* Li^+-G4, and the resulting speciation, local electrolyte structure (and dynamics). Starting with our first-level DFT analysis of LiTDI and LiTFSI ion-pairs (Figure 2a) this shows that both Li^+ and $[LiG4]^+$ have stronger interactions with TFSI than TDI, by 79 and 34 kJ mol^{-1}, respectively. These simple ion-pair models, however, fail to account for all coordination situations as well as the impact of triplet and aggregate formation, such as the importance of Li^+ coordination by the imidazolium nitrogen in the LiTDI-G4 system to stabilize higher aggregates.[16] The simplest larger model reaction to cover polyanion formation is the condensation of two $(LiG4)_2TDI_2$ to $[(LiG4)_2LiTDI_4]^-$ accompanied with the release of one Li^+ and two G4 (Figure 2b). In vacuum this is an endothermal process (+693 kJ mol^{-1}), but substantially less so than for two (LiG4)TFSI to $[LiTFSI_2]^-$ (+836 kJ mol^{-1}). The Li^+ and G4 released can be adopted by $(LiG4)_2TDI_2$ to form two $(LiG4)_2TDI$, (−600 kJ mol^{-1}) or by two (LiG4)TFSI to form $(LiG4)_3TFSI_2$, (−648 kJ mol^{-1}), respectively. Additional G4 are easily accommodated, making the electrolyte "softer" and thereby likely enhancing the ion transport (see also below). While the energies show some preference for TDI aggregation and TFSI to accept the released Li^+ and G4, the equilibrium is still shifted towards the reactant side by 45 kJ mol^{-1} (693–648 = 45), but this can be altered by a decreased G4 content, as emphasized in following total reaction [Eq. (1)]:

$$2(LiG4)_2TDI_2 + (LiG4)TFSI \rightleftharpoons [(LiG4)_2LiTDI_4]^- + [(LiG4)_2TFSI]^+ + G4 \quad (1)$$

In order to verify/dismiss the above picture, IR and Raman spectroscopies were applied and for the lowest total salt to solvent ratio (1 : 1) the spectra can be almost be considered as superpositions of the spectra of the mono-salt electrolytes (Figures 3 and S3). The main peak in all the Raman spectra is ν_{CN} at 2230 cm^{-1}, attributed to ion-pairs.[18] A minor difference is, however, observed at *ca.* 2260 cm^{-1}, where a shoulder starts to appear from $x_{TDI} = 0.3$, possibly indicating aggregated LiTDI. For the intermediate total salt content systems a distinct peak at 2257 cm^{-1} appears for $x_{TDI} = 0.4$, and furthermore has an

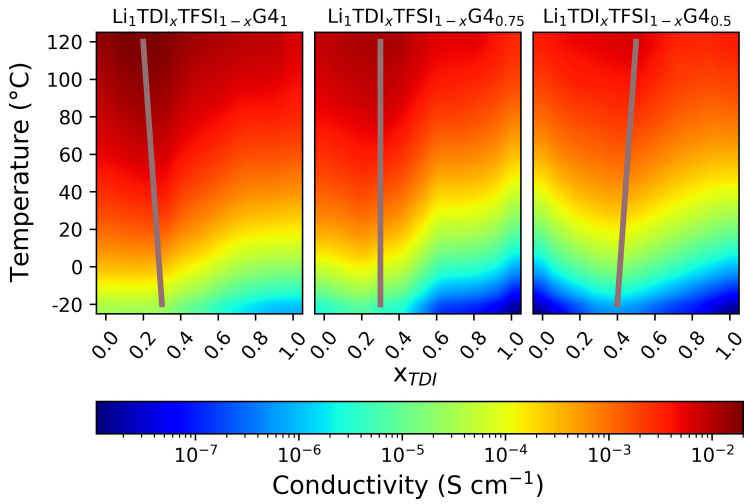

Figure 1. Heat-maps of ion conductivities as function of x_{TDI} and temperature for three different total salt contents. Brown lines indicate ridges of maximum ion conductivity.

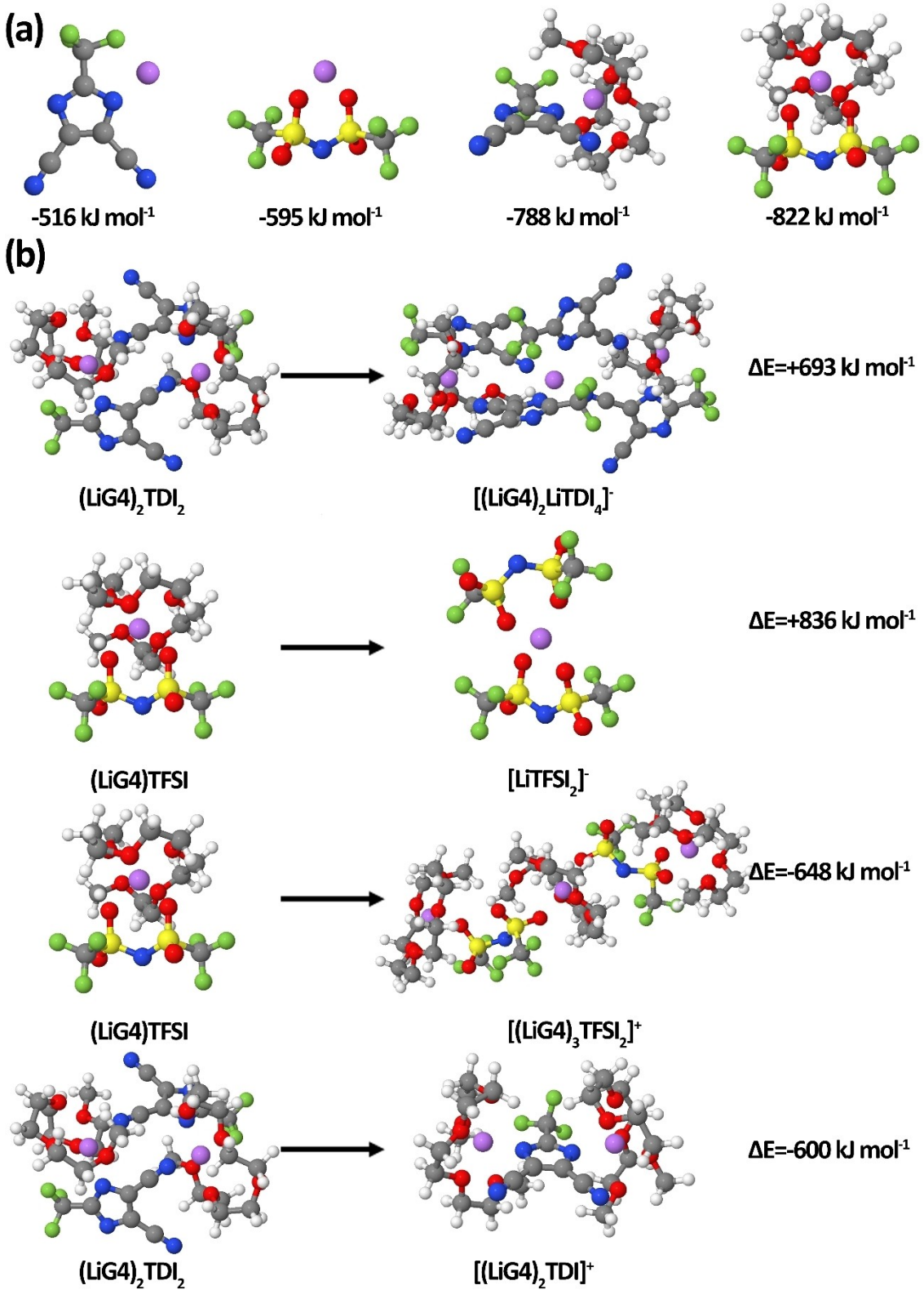

Figure 2. DFT-calculated structures and energies: a) most stable ion-pairs and b) disproportionation of anionic and cationic species.

additional shoulder at 2270 cm^{-1} for the highest total salt content systems – indicative of aggregated and highly aggregated forms of LiTDI, *i.e.* formation of polyanions for the TDI-richer systems. This is also visible in the FTIR spectra with even clearer signs of higher fractions of aggregates at lower LITDI concentrations (Figure S3). For TFSI, employing the "all-breathing mode" range 730–750 cm^{-1},[24] show a broad feature composed of at least two bands: solvent-separated ion-pairs at

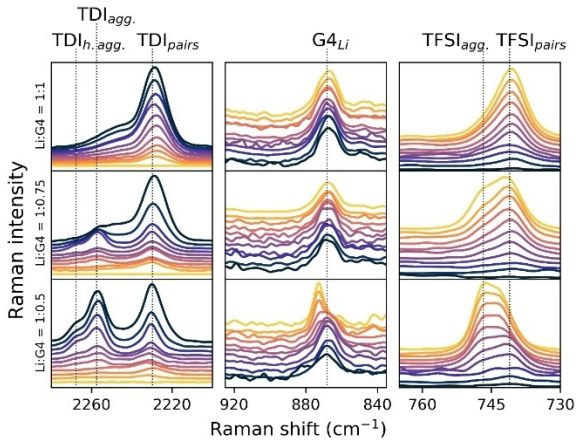

Figure 3. Raman spectra of electrolytes: Colours indicate x_{TDI}: $x_{TDI}=0$ in orange and $x_{TDI}=1.0$ in navy. Spectra shifted vertically for clarity.

741 cm^{-1} and aggregates at 747 cm^{-1}.[25] Again there are no visible changes the lowest total salt to solvent ratio (1:1) and some for both higher total salt content and when increasing x_{TDI} the peak at 741 cm^{-1} increases at the expense of the 747 cm^{-1} peak – and as the effect is strongest for the 1:0.5 system this supports the release of extra Li^+ as a result of TDI-based polyanion formation. This is also visible in the FTIR spectra; for both ν_{SC} (792 cm^{-1}) and the "all-breathing mode" (740 cm^{-1})[24] a shift of *ca.* 4 cm^{-1} is observed for the high concentrations of LiTFSI, which is not observed when LiTDI has been added. As expected there is no spectral feature from "free" G4, typically at *ca.* 840 cm^{-1}, but instead the combination band of CH_2 rocking and C–O stretching appears at 870 cm^{-1} – which is typical for a polyether chain conformation wrapped around a Li^+.[26,27] The sharper feature at *ca.* 875 cm^{-1}, which is uniquely present for the lower TDI concentrations of the most concentrated system, is a sign of a somewhat different interaction. This is corroborated by the CHAMPION analysis (discussed later) showing these to be somewhat similar, but not identical, to SILs (see Figures 4c and 5a below). Concluding this analysis; when LiTFSI is replaced by LiTDI in the electrolytes, the aggregation around TFSI is partially mitigated, but at the cost of a very rapid aggregation around TDI – in line with the trend in conductivity with a positive effect of a minor addition of LiTDI, altogether confirming our original hypothesis.

2.3. Global and Local structure, Dynamics, and Ion Transport

The final tool chosen to improve our understanding of the synergies between LiTDI and LiTFSI was MD simulations, using a set-up developed before.[16] First, the chelating effect of G4 results in ether oxygen atoms to dominate the Li^+ first solvation shell for the low total salt content systems (Figure S4 and S5), but this dominance decreases as function of both salt content and increasing x_{TDI}. This is related to the TDI-driven aggregation and the final concurrent release of Li^+. This can be observed as an average decrease in G4 coordination and the % of O_{ether} in the Li^+ first solvation shell ($r_{Li+\text{-}O}=2.5$ Å) can serve as an indicator of aggregation (Figure 4a–c). The least concentrated system (Li:G4 = 1:1) changes from mainly ion-pairs for $x_{TDI}=0$ to aggregates and "free" ions for $x_{TDI}=1$. The change is,

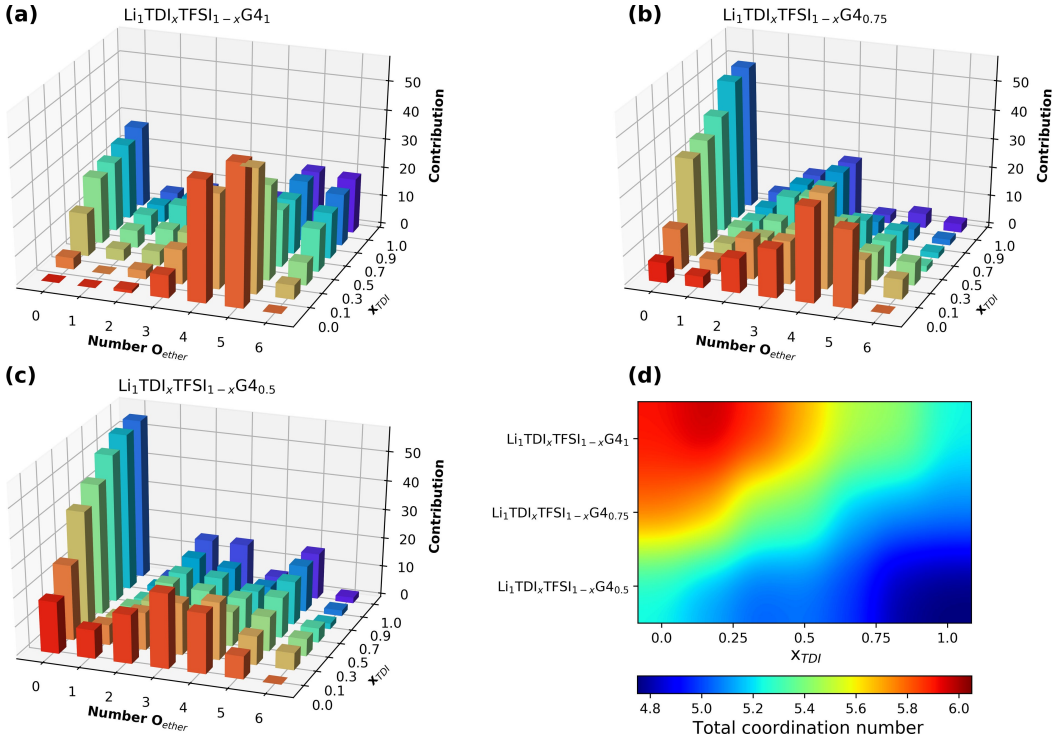

Figure 4. Distribution of O_{ether} in the Li^+ first coordination shell for different concentrations (a–c) and total CN of Li^+ (d).

however, not linear; the rate of change is larger for low x_{TDI} – already at $x_{TDI}=0.3$ 15% of the Li^+ are solely coordinated by anions. The 1:0.75 and 1:0.5 systems have even higher contents of aggregates, even without LiTDI present ($x_{TDI}=0$), but addition of LiTDI increases the amount of aggregates and, at least initially, "free" cationic species. For small G4 and TFSI contents, very few Li^+ coordinated by only one O_{ether} were found (Figure 4c). This can be considered as a consequence of the temporary nature of this coordination; we believe it occurs mainly during re-organization of aggregates, after which either the chelating effect acts to add more coordinating O_{ether} from G4 or the anions expel the last remaining O_{ether}. This matches very well with the observation of a narrower liquidus range from the DSC studies. Overall, the higher anion content in the first cation solvation shell, *i.e.* lower % O_{ether}, as a function of both total salt content and x_{TDI}, also lowers the total CN of Li^+ – from 5.91 for $Li_1TFSI_1G4_1$ to 4.74 for $Li_1TDI_1G4_{0.5}$ (Figure 4d).

To further investigate the global and local structure and the dynamics of these electrolytes, we analysed the MD simulation trajectories using CHAMPION[22,23] for the three systems with the lowest (equimolar, 1:1) salt concentrations: $x_{TDI}=0$, 0.3 and 1, in order to dynamically detect covalent and coordination bonds. Structurally, the pure LiTFSI system ($x_{TDI}=0$) overall clearly forms a SIL, as the cumulative distributions of Li^+ and G4 overlap perfectly for the Li^+-containing connected components (Figure 5a). While all Li^+ ions thus are solvated by G4, 80% of them also form ion-pairs and higher aggregates with TFSI with a maximum of 14 ions in total. At the other extreme, $x_{TDI}=1$, the majority, *ca.* 55%, of the Li^+ ions are part of a percolating anionic network with 1.2 TDI anions and 0.6 G4 solvent molecules per Li^+ (Figure 5c), rendering it negatively charged with a net charge density of -0.2 e/Li^+. For the minor components, 19% of the Li^+ ions do not coordinate to any TDI anions. In addition, and in contrast to the pure LiTFSI case above, only a negligible fraction of the Li^+ ions (1%) are solvated by a single G4, as discussed above. Clearly, this system does not qualify as a SIL.

The structure of the hybrid system ($x_{TDI}=0.3$, Figure 5b) is more similar to the LiTFSI system in that no percolating network is formed. While the cumulative distributions for Li^+ and G4 follow closely up to $n=10$, they by no means match perfectly, indicating a deviation from SIL behaviour. The size distribution of components is also intermediate.

For a more intuitive view of the network structures, some typical ionic aggregates are shown in Figure 6. The pure LiTFSI system forms flexible chains of alternating (G4 solvated) cations and anions (Figure 6a), which most often are linear but sometimes branched. The aggregate shown holds 7 Li^+ and 7 TFSI in total, whereof 6 Li^+ and 6 TFSI form a linear chain with a single ion-pair branching off from the main chain. This is the maximum number of ions observed in a single aggregate. Most of the chains in the system are, however, significantly shorter with single ions, monomers and dimers making up in total 70%. In stark contrast, the pure LiTDI system forms a more branched network structure (Figure 6c) made up of alternating naked Li^+ and TDI anions, where each branch is terminated whenever a Li^+ ion is solvated by one or more G4 molecules. Outside of this percolating network single ions and small components are found. The large aggregate shown in Figure 6b for the hybrid system ($x_{TDI}=0.3$) looks piecewise similar to the structures found in the pure systems, in line with the Raman and IR results; a LiTFSI chain of length 7 has a sidechain of length 2 which is immersed in a more TDI rich network structure. However, the lower concentration of TDI anions precludes formation of a percolating network as more of the Li^+ ions are solvated. This appearance of moderately aggregated LiTDI also corroborates the Raman and IR findings. As in the other systems, this is immersed in mostly smaller components, including single ions.

Turning to the details of the local structures, the G4 distribution is centred at 1 for all three electrolytes (Figure 7). From the SIL structure of the $x_{TDI}=0$ system, *i.e.* the pure LiTFSI system, the distributions broaden with an increasing proportion of LiTDI leading to progressively larger fractions of Li^+ with 0 and 2 solvating G4 molecules. The local structures are, however, strikingly different w.r.t. the anion distributions; the pure LiTFSI system has roughly equal fractions (*ca.* 40% each) of 1 and 2 TFSI per Li^+ with the remainder (*ca.* 20%) being solvent-separated ion-pairs (SSIPs) (Figure 7a), while the TDI distribution for the pure LiTDI system ($x_{TDI}=1$) in contrast is

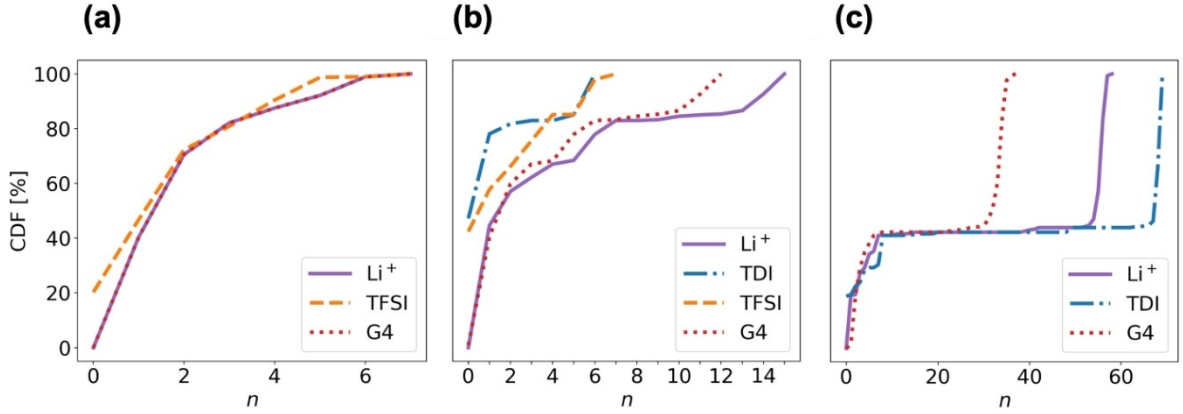

Figure 5. CDF based probability of Li^+ to be in a connected component with n ions/molecules for x_{TDI} = a) 0, b) 0.3, and c) 1.

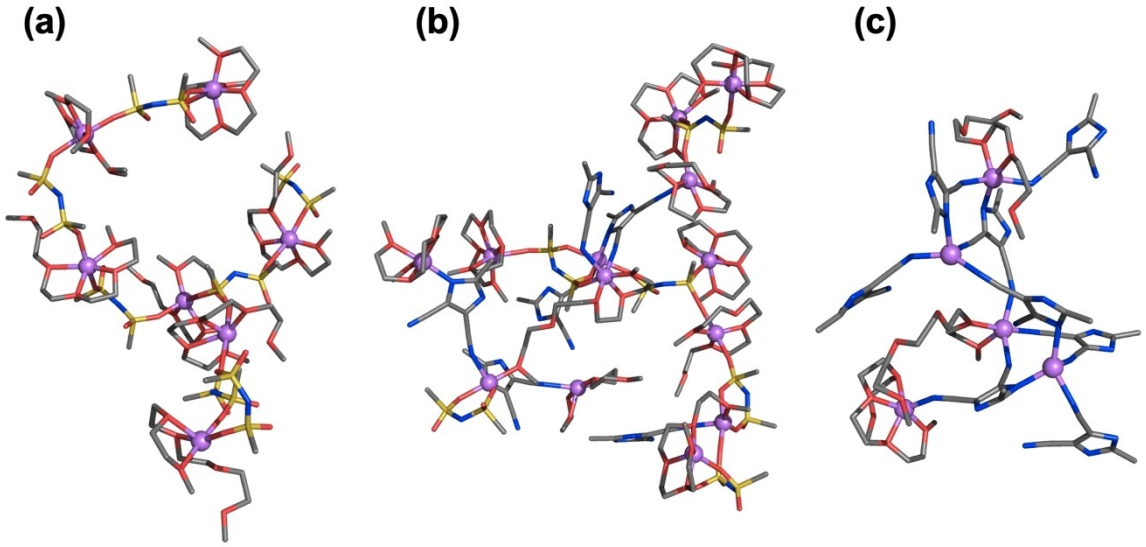

Figure 6. Examples of network structures formed in the three electrolytes x_{TDI} = a) 0, b) 0.3, c) 1. In (c) only a cut-out of the percolating network is shown. Element colours: Li: purple, C: grey, N: dark blue, O: red, S: yellow. The H and F atoms are omitted and the Li^+ ions are shown as spheres for greater visibility.

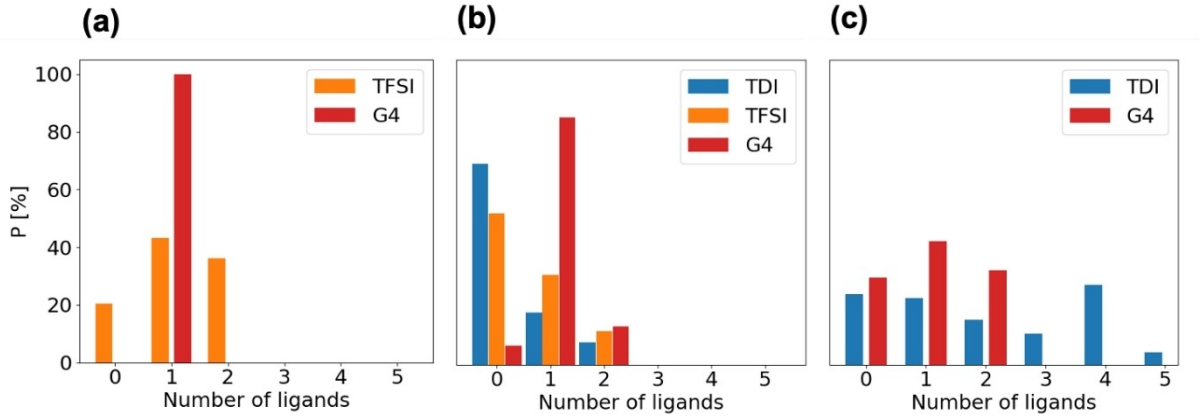

Figure 7. Li^+ ligand distributions for x_{TDI} = 0, 0.3 and 1.

bimodal and decreases from 23% for 0 to 10% for 3, but has a global maximum of 26% for 4 coordinated TDI ions, giving rise to a disproportionated structure (Figure 7c). In the hybrid system (x_{TDI} = 0.3) the distributions of both anions are pushed downward due to their competitive Li^+ coordination, giving 0.57 TFSI ions and 0.35 TDI ions on average in the Li^+ first solvation shell (Figure 7b). Overall, this analysis of the local structure is quite complementary and agree qualitatively with the one depicted in Figure 4, while numerically it differs due to the different methodologies applied.

The local structure around the Li^+ ions was further investigated by bond topology analysis discriminating between distinct topologies up to two bonds removed from a central Li^+ ion, but disregarding differences in the number of coordinated oxygen atoms in the G4 solvents, as long as the total number of G4 solvent molecules is the same. The four most frequent topologies account for 98% of the Li^+ ions in the pure LiTFSI system, and for all a G4 solvent molecule is wrapped around them (Figure. 8, top) and *ca.* 80% are also coordinated by TFSI ions. The coordination is predominantly mono rather than bidentate to TFSI. For the pure LiTDI system the six most common topologies together comprise 63% of the Li^+ ions (Figure 8, bottom), wherein the two most common topologies typify the disproportionated structure of this electrolyte, with a fifth of the Li^+ being solvated by two G4 molecules and another fifth coordinating four TDI ions (second and fifth topologies, which differ only by the number of nitrile *vs.* imidazole N atoms coordinated). In the hybrid system (x_{TDI} = 0.3, Figure 8, middle), where the six most common topologies account for 73% of the Li^+ ions, the $[LiG4]^+$ complex is the most common topology, slightly more common (25%) than in the pure LiTFSI electrolyte (20%). Adding the fourth most common topology, 32% of the Li^+ ions are found to be free from anion coordination, suggestive of higher ionic conductivity as compared to systems with lower fractions of free ions. Indeed, based on the net charge distributions of Li^+ containing connected components (Figure S6), their average net charge is 0.72 in the hybrid system, compared to 0.37 in the pure LiTFSI

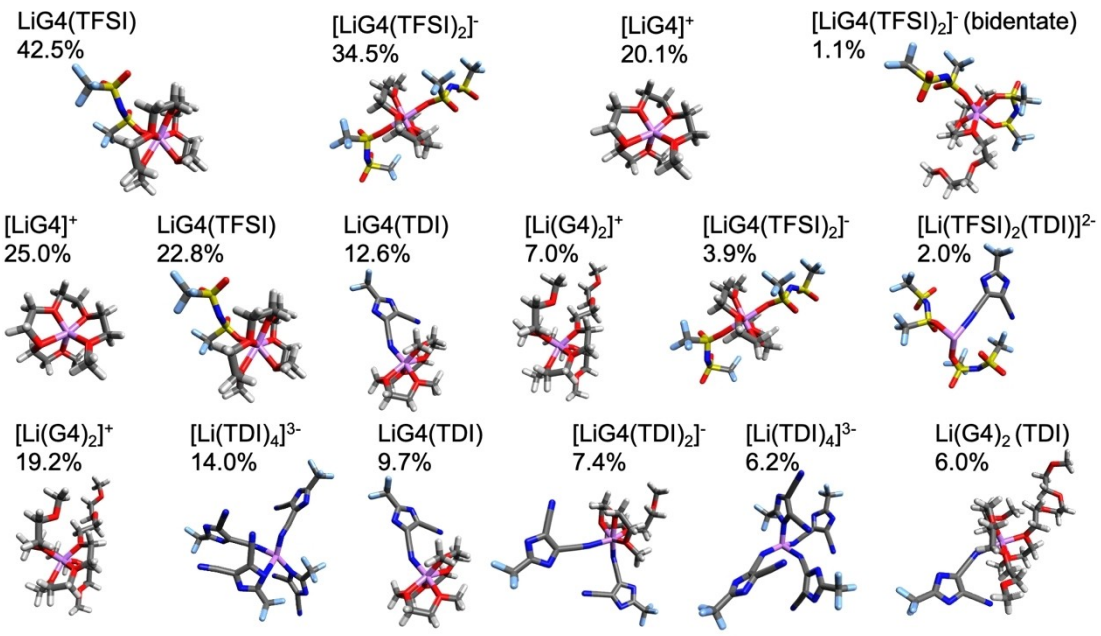

Figure 8. The most common Li^+ first solvation shell topologies for $x_{TDI} = 0$ (top), 0.3 (centre), and 1 (bottom). Element colours: H: white, Li: purple, C: grey, N: dark blue, O: red, F: light blue, S: yellow.

system and 0.60 for the 45% of Li^+ not part of the percolating network in the pure LiTDI system. That the hybrid system has a higher fraction of SSIPs than the pure LiTFSI system can be understood by its lower TFSI concentration combined with the higher interaction energies between Li^+ and TFSI as compared to Li^+ and TDI (*cf.* DFT results above).

The diffusive ion transport at steady state was investigated by the MSDs and as opposed to what could be expected from the ionic conductivies the diffusivities of both cations and anions decrease monotonically as functions of the LiTDI fraction, while the Li^+ transport numbers do not change significantly (Figure 9). This can, at least in part, be explained by the higher concentration of Li^+ ions not coordinated to anions in the hybrid system as compared to both the pure systems, which is consistent with the higher t^+ in the hybrid system (albeit within the margin of error). By computing the correlations between the effective diffusivities and the number of anions and G4 oxygen atoms in the Li^+ first solvation shell for the two pure systems, we obtain correlation coefficients of −0.76 and −0.67 and +0.57 and +0.84, respectively. This further strengthens the case for the G4 solvated, but anion free, Li^+ ions being important contributors to the cation transport.

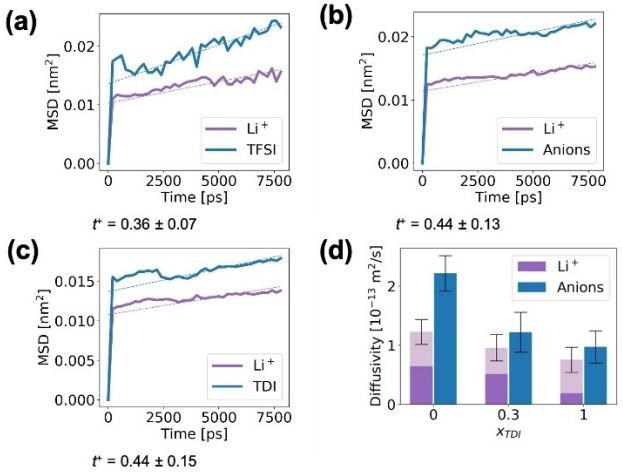

Figure 9. MSDs and transport numbers for $x_{TDI} =$ a) 0, b) 0.3 and c) 1, and d) diffusivities of Li^+ (decomposed into vehicular (dark) and structural (light) contributions) and anions for these electrolytes.

An important aspect of the Li^+ ion transport is whether it is vehicular *vs.* structural (non-vehicular) in nature, *i.e.* here the extent to which the Li^+ motion is correlated with the centre-of-mass motion of its component. For both the pure LiTFSI and the hybrid electrolytes, slightly more than half, 53% and 54%, respectively, of the diffusive Li^+ transport is vehicular w.r.t connected components, whereas only 25% is vehicular for the pure LiTDI system (Figure 9). This difference is logical considering the more or less immobile percolating network in the latter system and hence the Li^+ transport should be more dependent on structural rearrangements. From the point of view of the Li^+ first solvation shell, roughly 85% of the diffusivity is vehicular for all three electrolytes, further strengthening that the main difference in ion transport mechanism for the LiTDI system is the contribution from structural changes of large structures, rather than changes in the cation first solvation shell.

3. Conclusions

Altogether, a hybrid/mixed LiTDI/LiTFSI system has the potential to outperform mono-salt systems by combining the disproportionation reaction creating polyanions and "free" cationic species with balancing the creation of highly aggre-

gated structures and sustain the dynamics. The optimum is achieved by a small addition of LiTDI to a LiTFSI-based electrolyte – shown here for different HCEs as a decreased solvent content makes the effects more pronounced. As can be seen from the conductivity data, however, the effect on the ion transport mechanism is general across all the systems. Yet, while the diffusivities of both Li^+ and anions decrease monotonically with the fraction of LiTDI due to more aggregation the maximum in ionic conductivity for small amounts of LiTDI can be attributed to a higher fraction of free and relatively mobile Li^+ ions. That is possibly also associated with a modest increase in the cation transport number – yet within the statistical uncertainty the anion contribution is on par for $x_{TDI} = 0.3$ and 1, while clearly dominant for $x_{TDI} = 0$. From this combined, novel more performant electrolytes can in a very general sense be designed by making use of the above balance *e.g.* by using LiTDI, or any other salt capable of combining a disproportionation reaction with the creation of highly aggregated structures, as an additive/co-salt.

Acknowledgements

All DFT calculations and MD simulations were carried out at the Wrocław Centre for Networking and Supercomputing, Grant 346. We are grateful for the financial support from the Swedish Energy Agency by the projects within "Batterifondsprogrammet": "Next Generation Batteries" (#37671-1) and "Highly Concentrated Electrolytes" (#39909-1) as well as the funding received through the European Union's Horizon 2020 research and innovation program under Grant Agreement No. 666221 (HELIS). The continuous support to P.J. from several of Chalmers Areas of Advance: Materials Science, Energy, and Transport, is also gratefully acknowledged, and especially the support to R.A. within the Theory and Modelling scheme of Advanced User Support from the Chalmers Area of Advance: Materials Science.

Conflict of Interest

The authors declare no conflict of interest.

Keywords: Bi-salt system · Concentrated electrolytes · Conductivity · Lithium · Modelling

[1] K. Xu, *Chem. Rev.* **2014**, *114*, 11503–11618.
[2] D. Aurbach, Y. Talyosef, B. Markovsky, E. Markevich, E. Zinigrad, L. Asraf, J. S. Gnanaraj, H.-J. Kim, *Electrochim. Acta* **2004**, *50*, 247–254.
[3] F. Huang, G. Ma, Z. Wen, J. Jin, S. Xu, J. Zhang, *J. Mater. Chem. A* **2018**, *6*, 1612–1620.
[4] S. Wilken, P. Johansson, P. Jacobsson, in *Lithium Batteries* (Eds.: B. Scrosati, K. M. Abraham, W. V. Schalkwijk, J. Hassoun), John Wiley & Sons, Inc., **2013**, pp. 39–70.
[5] H. Zhang, U. Oteo, X. Judez, G. G. Eshetu, M. Martinez-Ibañez, J. Carrasco, C. Li, M. Armand, *Joule* **2019**, *3*, 1689–1702.
[6] P. Jankowski, W. Wieczorek, P. Johansson, *Phys. Chem. Chem. Phys.* **2016**, *18*, 16274–16280.
[7] W. Gorecki, M. Jeannin, E. Belorizky, C. Roux, M. Armand, *J. Phys. Condens. Matter* **1995**, *7*, 6823.
[8] L. Niedzicki, G. Z. Żukowska, M. Bukowska, P. Szczeciński, S. Grugeon, S. Laruelle, M. Armand, S. Panero, B. Scrosati, M. Marcinek, W. Wieczorek, *Electrochim. Acta* **2010**, *55*, 1450–1454.
[9] A. Plewa-Marczewska, T. Trzeciak, A. Bitner, L. Niedzicki, M. Dranka, G. Z. Żukowska, M. Marcinek, W. Wieczorek, *Chem. Mater.* **2014**, *26*, 4908–4914.
[10] A. Boschin, P. Johansson, *Electrochim. Acta* **2015**, *175*, 124–133.
[11] Z. Ma, M. Kar, C. Xiao, M. Forsyth, D. R. MacFarlane, *Electrochem. Commun.* **2017**, *78*, 29–32.
[12] Y. Yamada, A. Yamada, *J. Electrochem. Soc.* **2015**, *162*, A2406–A2423.
[13] K. Ueno, K. Yoshida, M. Tsuchiya, N. Tachikawa, K. Dokko, M. Watanabe, *J. Phys. Chem. B* **2012**, *116*, 11323–11331.
[14] T. Tamura, K. Yoshida, T. Hachida, M. Tsuchiya, M. Nakamura, Y. Kazue, N. Tachikawa, K. Dokko, M. Watanabe, *Chem. Lett.* **2010**, *39*, 753–755.
[15] T. Mandai, K. Yoshida, K. Ueno, K. Dokko, M. Watanabe, *Phys. Chem. Chem. Phys.* **2014**, *16*, 8761–8772.
[16] P. Jankowski, M. Dranka, W. Wieczorek, P. Johansson, *J. Phys. Chem. Lett.* **2017**, *8*, 3678–3682.
[17] P. Jankowski, M. Dranka, G. Z. Żukowska, J. Zachara, *J. Phys. Chem. C* **2015**, *119*, 9108–9116.
[18] P. Jankowski, M. Dranka, G. Z. Żukowska, *J. Phys. Chem. C* **2015**, *119*, 10247–10254.
[19] M. J. Frisch, G. W. Trucks, H. B. Schlegel, G. E. Scuseria, M. A. Robb, J. R. Cheeseman, G. Scalmani, V. Barone, B. Mennucci, G. A. Petersson, H. Nakatsuji, M. Caricato, X. Li, H. P. Hratchian, A. F. Izmaylov, J. Bloino, G. Zheng, J. L. Sonnenberg, M. Hada, M. Ehara, K. Toyota, R. Fukuda, J. Hasegawa, M. Ishida, T. Nakajima, Y. Honda, O. Kitao, H. Nakai, T. Vreven, J. A. Montgomery Jr., J. E. Peralta, F. Ogliaro, M. J. Bearpark, J. Heyd, E. N. Brothers, K. N. Kudin, V. N. Staroverov, R. Kobayashi, J. Normand, K. Raghavachari, A. P. Rendell, J. C. Burant, S. S. Iyengar, J. Tomasi, M. Cossi, N. Rega, N. J. Millam, M. Klene, J. E. Knox, J. B. Cross, V. Bakken, C. Adamo, J. Jaramillo, R. Gomperts, R. E. Stratmann, O. Yazyev, A. J. Austin, R. Cammi, C. Pomelli, J. W. Ochterski, R. L. Martin, K. Morokuma, V. G. Zakrzewski, G. A. Voth, P. Salvador, J. J. Dannenberg, S. Dapprich, A. D. Daniels, Ö. Farkas, J. B. Foresman, J. V. Ortiz, J. Cioslowski, D. J. Fox, *Gaussian 16, Revision B.01*, Gaussian, Inc., Wallingford, CT, USA, **2016**.
[20] M. J. Abraham, T. Murtola, R. Schulz, S. Páll, J. C. Smith, B. Hess, E. Lindahl, *SoftwareX* **2015**, *1–2*, 19–25.
[21] N. Michaud-Agrawal, E. J. Denning, T. B. Woolf, O. Beckstein, *J. Comput. Chem.* **2011**, *32*, 2319–2327.
[22] R. Anderson, F. Årén, A. A. Franco, P. Johansson, *In manuscript*.
[23] R. Anderson, F. Årén, A. A. Franco, P. Johansson, *Submitted to Journal of the Electrochemical Society*.
[24] I. Rey, P. Johansson, J. Lindgren, J. C. Lassègues, J. Grondin, L. Servant, *J. Phys. Chem. A* **1998**, *102*, 3249–3258.
[25] L. Suo, F. Zheng, Y.-S. Hu, L. Chen, *Chinese Phys. B* **2016**, *25*, 016101.
[26] J.-K. Hyun, H. Dong, C. P. Rhodes, R. Frech, R. A. Wheeler, *J. Phys. Chem. B* **2001**, *105*, 3329–3337.
[27] H. Matsuura, K. Fukuhara, *J. Polym. Sci. B* **1986**, *24*, 1383–1400.

Manuscript received: August 8, 2020
Revised manuscript received: September 8, 2020
Accepted manuscript online: September 10, 2020
Version of record online: October 1, 2020